



Multi-products (C1 and C2) Formation from Electrochemical Reduction of Carbon Dioxide Catalyzed by Oxide-Derived Coppers Prepared Using Varied Synthesis Conditions

Madhurima Barman^{1,2} · Venkata Sai Sriram Mosali² · Alan M. Bond² · Jie Zhang² · A. Sarkar¹

Accepted: 30 January 2023 / Published online: 13 February 2023

© The Author(s), under exclusive licence to Springer Science+Business Media, LLC, part of Springer Nature 2023

Abstract

In order to explore the effects of morphology, specific surface area and relative content of Cu/Cu-oxide in “CuO-derived Cu” electrocatalysts on the current density and product formation during electrochemical carbon dioxide reduction reaction (eCO₂RR), CuO electrocatalysts were synthesized via solution combustion and hydrothermal routes, possessing different morphologies. The as-synthesized CuOs were first reduced to Cu at -0.8 V (vs. RHE), till the currents got stabilized; thus, forming “CuO-derived Cu”. Subsequently, eCO₂RR was carried out via bulk electrolysis at different potentials between -0.6 and -1.6 V (using 0.1 M KHCO₃ solution), leading to the formation of seven liquid/gaseous products, viz., CO, methane, ethylene, formate, acetate, and ethanol (in addition to H₂). It was interesting to note that the type of products and associated faradic efficiencies (FEs) were governed by the Cu-content of the “CuO-derived Cu” electrocatalysts (i.e., Cu:CuO ratio), as obtained post the pre-reduction step and looked into here as one of the starting conditions of the electrocatalysts. Higher initial Cu-content of the pre-reduced CuOs resulted in higher FEs at lower negative potentials. Furthermore, high Cu-content (even for simple equiaxed morphology), as opposed to any special morphology (say, rod/whisker-type), has been found to be particularly important for the formations of methane and formate; yielding a maximum FE of $\sim 18.6 \pm 1.2\%$ at -1.0 V for the latter. Accordingly, the present work reveals the relative roles of specific surface area and Cu/CuO-content of “CuO-derived Cu” electrocatalysts on the current densities, product formation and associated FEs on eCO₂RR.

Keywords Electrochemical CO₂ reduction · CuO-derived Cu electrocatalysts · Morphology · Specific surface area · Cu/CuO ratio

Introduction

Electrochemical reduction of carbon dioxide (eCO₂RR) is one of the promising techniques to mitigate the unwanted greenhouse gas (CO₂), while at the same time convert CO₂ to useful chemicals and fuels. More conventionally, metallic materials, such as Au, Ag, Cu, Pb, Ni, Fe, Zn, and Sn, have been in use as electrocatalysts for eCO₂RR [1–6]. More

recently, metallic alloy [7–9], metal oxides [10–13], and metal oxide composites [14–16] are being investigated as potential electrocatalysts. The oxides may have advantages over the metallic counterparts, in terms of being tunable and dopable, presenting a wider selection of catalyst for the eCO₂RR process [17, 18]. The commonly obtained products of eCO₂RR include CO, CH₄, C₂H₄, HCOO⁻ (formate), CH₃COO⁻ (acetate), C₂H₅OH, n-propanol etc.; the type(s) and their relative amount(s) depends on binding strength/mode of CO₂/CO intermediate on the surface of catalysts [2], in addition to the reaction conditions. Undoubtedly, the type/efficiency of the product formation and the associated adsorption/desorption mechanisms are expected to depend critically on the electrocatalysts used, in terms of composition, morphology, surface area and binding energy with CO₂/CO/other intermediates [11, 14, 19–24].

Copper, as electrocatalysts for eCO₂RR, reduces CO₂ to form a lot of multi-carbon products due to its intermediate CO-binding energy [5, 7, 8, 25–27] for eCO₂RR among all

✉ Jie Zhang
Jie.Zhang@monash.edu

✉ A. Sarkar
a.sarkar@iitb.ac.in

¹ Reaction Engineering and Catalysis Laboratory, Department of Chemical Engineering, Indian Institute of Technology Bombay, Mumbai, India

² School of Chemistry, Monash University, Clayton Campus, Melbourne, VIC, Australia

metals. Hori et al. [1] reported the formation of six different hydrocarbon products using 0.10 M KHCO_3 electrolyte. More recently, Kuhl et al. [5] was able to obtain 16 different products upon eCO_2RR using 0.10 M KHCO_3 solution with a pH of 6.8 (i.e., pH of 6.8 after CO_2 purging). Oxide derived Cu possesses a higher activity and product selectivity due to the presence of grain boundary [28, 29] and/or metastable oxides [13, 22, 30, 31] although there has been some debate over the stability of copper oxides under eCO_2RR conditions [29, 31–34]. The above renders it advantageous to start with copper oxides; with an added possibility of them being partly/fully electrochemically reduced to the metallic form in situ during the initial (or pre-) stages of eCO_2RR [31, 32] and, thus, harness the advantages of the metallic form, as well. Literature on eCO_2RR using CuO claim that the metal oxide can be potentially reduced to the metallic form during eCO_2RR [21, 35]; thus, forming copper oxide derived copper (“CuO-derived Cu”) [18–21, 23, 24, 28, 29, 32–34, 36–40]. Furthermore, as also reported by our group [41], “CuO-derived Cu” is more efficient as an electrocatalyst than polycrystalline Cu; and can lead to the formation of formate ions as the product of eCO_2RR in 0.5 M NaHCO_3 . In the context of oxide-derived Cu electrocatalysts, more recent studies have also talked and debated about the possible importance(s) of the morphology of CuO and the extent of CuO reduction prior to eCO_2RR (in terms of oxidation states of Cu) [18, 25–27, 33, 36, 37]. Furthermore, the usage of mixed CuO/Cu electrocatalysts for eCO_2RR has also been looked into in terms of the associated selectivity towards product formation [30, 42]. In fact, it has also been observed (including with *operando* techniques) that some residual Cu-oxide exists (and appears to be fairly stable) along with Cu during eCO_2RR , even at highly negative potentials [31–34].

However, the possible effect(s) of the synthesis route and/or morphology of CuO on the degree of electrochemical reduction of the same during a pre-reduction electrolysis and, in turn, the influence of the as-generated Cu/CuO content(s) on the subsequent eCO_2RR have not been reported yet. In more specific terms, the present literature base lacks a systematic set of study and information pertaining to the possible effect(s) of starting morphology and specific surface area of CuO-based electrocatalysts on the evolution of metallic Cu during electrochemical CO_2 reduction (or pre-reduction step) and the influence of the same, along with specific surface area, toward the current density, type of product(s) formed and the associated faradaic efficiencies. This is despite the fact that the synthesis process of CuO is fairly facile and cost-effective; which also renders varying the morphology and surface area during synthesis feasible, even in the practical context.

Accordingly, in the present work, CuO electrocatalysts, possessing different morphologies (viz., rod/whisker-type or simple equiaxed) and surface areas were synthesized via

solution combustion and hydrothermal routes (with varied conditions/precursors), which were then electrochemically reduced to form “CuO-derived Cu”. When used for eCO_2RR via bulk electrolysis (using 0.10 M KHCO_3 solution) at six different potentials in the range of -0.6 to -1.6 V vs. RHE; the “CuO-derived Cu” electrocatalysts yielded different current densities and types/amounts of products (viz., eight gaseous/liquid products, in total). Interestingly, the type/efficiency of product formation of eCO_2RR seems to have been governed partially by the Cu-content (i.e., Cu:CuO ratio) of the “CuO-derived Cu” electrocatalysts, as obtained post the pre-reduction step and prior to the actual eCO_2RR (i.e., as a starting condition of the electrocatalysts). Such a revelation concerning the influence of morphology of CuO on the Cu-content of pre-reduced “CuO-derived Cu” electrocatalysts and, in turn, on the performances as electrocatalysts for eCO_2RR , is expected to aid the selection, development and proper usage of CuO to cater to the requirements of/from the electrochemical CO_2 reduction process.

Experimental Details

Copper Oxide Synthesis Routes

Five different routes/protocols were followed for the synthesis of copper oxide catalysts; as described in the following and categorized as samples- 1 (S1), 2 (S2), 3 (S3), 4 (S4), and 5 (S5).

Sample 1 (S1)

The synthesis route adopted in this case was “citrate solution combustion”, with the precursors being copper nitrate trihydrate ($\text{Cu}(\text{NO}_3)_2 \cdot 3\text{H}_2\text{O}$; 99% pure; from Merck, India) and citric acid monohydrate ($\text{C}_6\text{H}_8\text{O}_7 \cdot \text{H}_2\text{O}$; 99.5% pure; from Merck, India). For preparing the aqueous solution, Millipore water (18.2 M Ω .cm) was used. Saturated aqueous solution of copper nitrate was mixed with citric acid (as fuel) in 1:1 molar ratio in a glass beaker, which was then placed on a hot plate at 120 °C with continuous stirring at 250 rpm until the formation of gel. After this, the temperature of the hot plate was increased to 250 °C, and the gel expanded to form “ash”. The as-synthesized “ash” was ground in an agate mortar-pestle and taken in a quartz boat for calcination in air at 750 °C for 2 h, with the heating rate being 10 °C/min. The as-synthesized and calcined CuO powder was black in color.

Sample 2 (S2)

The route adopted in this case, and also for samples S3, S4, and S5, was hydrothermal synthesis, but with varied

conditions and precursor types. In the cases of S2 and S3, copper nitrate trihydrate ($\text{Cu}(\text{NO}_3)_2 \cdot 3\text{H}_2\text{O}$; 99% pure; from ACROS Organics, USA) and sodium hydroxide (NaOH; 99% pure; from Merck, Germany) were used as the precursors. For S2, aqueous solution of sodium hydroxide (0.2 M) was added drop wise to the copper nitrate solution in 1:4 molar ratio under constant stirring at room temperature. After 30 min of stirring the blue colored solution was transferred to 80-ml Teflon lined stainless steel autoclave and heated at 180 °C for 5 h in an oven, to obtain the black colored precipitate.

Sample 3 (S3)

In the case of S3, the sodium hydroxide solution was added drop wise to copper nitrate trihydrate solution in 1:1 molar ratio under constant stirring at room temperature. After mixing for 30 min at room temperature, the blue colored solution was transferred to 80-ml Teflon lined stainless steel autoclave and the reaction was conducted at 180 °C, but for 24 h, yielding the black colored precipitate.

Sample 4 (S4)

In the case of S4, aqueous solution of 0.06 M copper acetate monohydrate ($\text{Cu}(\text{CO}_2\text{CH}_3)_2 \cdot \text{H}_2\text{O}$; 99% pure; from Sigma Aldrich), 0.1 M CTAB ($\text{C}_{19}\text{H}_{42}\text{BrN}$; 99% pure; from Sigma Aldrich) and 0.5 M sodium hydroxide (NaOH; 99% pure; from Merck, Germany) was stirred for 30 min at room temperature. The homogeneous solution was transferred to 80-ml Teflon lined stainless steel autoclave and placed in an oven at 180 °C for 16 h, to obtain the black colored precipitate.

Sample 5 (S5)

In the case of S5, 2 mM copper nitrate trihydrate ($\text{Cu}(\text{NO}_3)_2 \cdot 3\text{H}_2\text{O}$; 99% pure; from ACROS Organics, USA), 5 mM urea ($\text{Co}(\text{NH}_2)_2$; 99.5%; from Merck, Germany), and 3 mM CTAB ($\text{C}_{19}\text{H}_{42}\text{BrN}$; 99% pure; from Sigma Aldrich) were added to Millipore water (18.2 M Ω) and continuously stirred for 30 min at room temperature. The homogeneous solution was transferred to a Teflon lined stainless steel autoclave and heated at 180 °C for 6 h in an oven, yielding the black colored precipitate.

The black colored precipitates, obtained at the end of each of the above synthesis routes/conditions, were centrifuged and washed with Millipore water and ethanol several times. Then they were dried overnight at 70 °C and ground in an agate mortar pestle.

Material Characterizations

Phase evolution of the copper oxide samples synthesized using the five different routes/protocols (i.e., S1, S2, S3, S4, and S5) was checked with X-ray diffraction (XRD), using Bruker D8 Eco powder diffractometer with Cu K α radiation having $\lambda = 0.15406$ nm. The same was done also after preparing the “CuO-derived Cu” as catalysts for the electrochemical CO₂ reduction experiments. Inorganic Crystal Structure Database (ICSD) was used for the phase analysis of the powder catalysts. Fullprof suite software was used for the Rietveld refinement and Verta software for generating a view of the crystal structure. Morphologies of the oxide particles before and after pre-reduction were observed using scanning electron microscopy (SEM; FEI Magellan 400 FEGSEM). The specific surface area of the oxide catalysts was measured with BET (Brunauer–Emmett–Teller), using Micromeritics 3 FLEX surface characterization. In order to re-confirm the elemental composition and determine the oxidation state of Cu, X-ray photoelectron spectroscopy (XPS) was conducted with Al K α monochromatic radiations in a Kratos AXIS-supra analytical system. Surface charge correction of the scanned binding energies of the elements was performed with adventitious carbon C 1 s (C–C) at the binding energy of 284.8 eV. The high-resolution scans were deconvoluted using the XPSPEAK41 database.

Electrode Fabrication

Glassy carbon plates of 1.5 × 2.0 cm² dimensions were coated uniformly with one of the copper oxide catalysts (i.e., S1/S2/S3/S4/S5). The working electrode was prepared using 4:1 molar ratio of Millipore water and acetone (in 1-ml solution), 14 mg of copper oxide catalyst (S1/S2/S3/S4/S5) and 60 μL of basic nafion (5 wt.%) (as binder; from Merck). These were taken in a centrifuge tube and sonicated for 30 min. The as-prepared dispersed suspension is referred to as “ink”, which was drop-casted uniformly using 200- μL pipette on both sides of polished glassy carbon (GC) plate. The GC electrode was then kept under IR lamp for drying. The catalyst loading on the GC support was ~ 2.8 mg/cm². Basic solution of 0.10 M potassium bicarbonate (KHCO_3 ; ACS grade; from Merck) was used as the electrolyte, with both the compartments of the H-cell being filled with 10 ml of the same, leaving headspace volume of 20 ml in each compartment free. In order to electrochemically prepare the oxide derived copper catalyst, a potential of -0.8 V vs. RHE was applied either for 30 min (minimum) or till the current got stabilized (i.e., pre-reduction step).

Table 1 The lattice parameters and unit cell volumes of the CuO electrocatalysts, designated as S1, S2, S3, S4, and S5, as obtained upon Rietveld refinement of the corresponding XRD patterns

Serial number	The electrocatalysts	Lattice parameters (Å)			Unit cell volume, V (Å ³)
		a	b	c	
(a)	S1	4.68823(6)	3.42617(4)	5.13398(6)	81.354(2)
(b)	S2	4.68334(41)	3.42620(34)	5.13025(51)	81.178(13)
(c)	S3	4.68127(42)	3.42272(34)	5.12700(51)	81.005(13)
(d)	S4	4.69544(61)	3.42469(52)	5.12702(73)	81.342(20)
(e)	S5	4.67156(76)	3.42045(64)	5.11835(94)	80.639(25)

Underpotential Deposition of Pb on the “CuO-Derived Cu” Electrocatalysts

For the conducting underpotential deposition (UPD) and stripping experiments, the procedure described in two of our previously reported works [43, 44] has been followed. In more specific terms, the “CuO-derived Cu” electrocatalysts (S1 to S5), post the pre-reduction step at -0.8 V vs. RHE, have been subjected to 10 cycles of cyclic voltammetry scans between 0.7 and -1.1 V vs. RHE at a potential scan rate of 10 mV/s (using a PARSTAT 3000A potentiostat). In order to conduct the UPD of Pb on Cu, the electrolyte solution used has been Ar saturated 0.01 M HClO₄ (Perchloric acid 60%; ACS grade; from Merck) + 1 mM PbCl₂ (Lead Chloride (Anhydrous) 98% from LOBA Chemie).

The representative CVs obtained with the electrocatalysts, along with indication of the current peaks associated with the deposition and stripping of Pb monolayer, has been presented in Fig. S1 in the Supporting Information file (SI). It is the area under the peak corresponding to the Pb monolayer stripping during the anodic half cycle that has been used for estimating the electrochemically accessible/active specific surface areas, as per the procedure detailed in our previous publications [43, 44], where it was also reported that for monolayer deposition/stripping of Pb on polycrystalline Cu, the average amount of charge transferred is 250 $\mu\text{C}/\text{cm}^2$.

Electrochemical CO₂ Reduction

Gas tight two compartment electrolysis cell (H-shaped; viz., “H-cell”) was used for carrying out the electrochemical carbon dioxide reduction reactions (see Fig. S2 in SI). The two compartments of the H cell, i.e., the anode and cathode chambers were separated by porous glass frit separator. Three electrodes (viz., working, counter, and reference) were used during the experiment. Copper-modified electrode fabricated according to the procedure described in the “[Electrode Fabrication](#)” section was used as the working electrode, Pt-mesh was used as the counter and Ag/AgCl (1 M) was used as the reference electrode. The potential of the Ag/AgCl (1 M) reference electrode is 0.222 vs. standard hydrogen electrode. The potential applied using Ag/AgCl (1.0 M

KCl) reference electrode was converted to the RHE scale as per, $E_{\text{RHE}} = E_{\text{Ag/AgCl}} + 0.222$ (V) + 0.0586 (V) \times pH (22 °C).

Prior to performing eCO₂RR, high purity carbon dioxide (CO₂) was purged into the electrolyte for at least 30 min and pH of the CO₂ saturated electrolyte was maintained at 6.8. The aqueous solutions in both the compartments were stirred during the CO₂ purging step, as well as during the bulk electrolysis (i.e., CO₂ reduction) experiment. Electrochemical CO₂ reduction reaction was performed via bulk electrolysis technique at room temperature (22 ± 2 °C) using CHI 760D electrochemical workstation (CH Instruments, Austin, TX, USA). Then potentials of -0.6 , -0.8 , -1.0 , -1.2 , -1.4 and -1.6 V vs. RHE (iRu effect was not corrected) were applied for the CO₂ reduction reaction via bulk electrolysis until 10 C of charge was consumed for each reaction at a given potential. The current was monitored as a function of time during the experiments.

Product Analysis

After the bulk electrolysis experiments, 200 μL of the gaseous product samples were collected using a gas-tight syringe from the headspace of the cathode compartment and analyzed

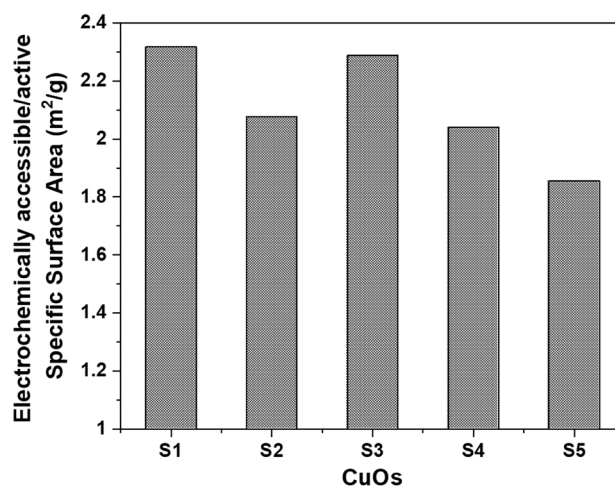


Fig. 1 Electrochemically accessible/active specific surface areas of the as-synthesized (-cum-calcined) copper oxide powder samples, designated as S1, S2, S3, S4, and S5, as obtained based on the underpotential deposition (UPD) measurements

by gas chromatography (GC). H_2 was analyzed using Agilent gas chromatography (7820A), with a thermal conductivity detector (TCD), column length of 24 m, HP-plot molesieve (5 \AA) and carrier gas as N_2 . CO was analyzed using Agilent gas chromatography (7820A), with a thermal conductivity detector (TCD), column length of 4 m, HP-plot molesieve (5 \AA), and carrier as He. C_2H_4 was analyzed using Agilent gas chromatography (7820A), with a flame ionization detector (FID), column length of 30 m, HP-5 (nonpolar), and carrier gas as N_2 .

The liquid products were analyzed with nuclear magnetic resonance (NMR) spectroscopy (using BRUKER ULTRASHIELD 600 PLUS NMR spectrometer), having an operational frequency of 600 MHz in order to obtain 1H NMR spectra. For the NMR analysis, sample preparation

involved using 0.6 ml of the electrolyte (post electrolysis), mixed with 100 μL of deuterium oxide (D_2O ; 99.9 at. % D; from Cambridge Isotope Laboratories Inc.) and 100 μL of dimethyl sulfoxide (DMSO; 99.9%; from Merck, Japan), diluted to 100 ppm (v/v) by water prior to use, in the NMR tube. All the samples were measured three times to obtain the mean and standard deviation.

Results and Discussion

The As-Synthesized CuO Samples

As per the focus of this work, copper oxide (CuO) electrocatalysts were synthesized following five different protocols, with

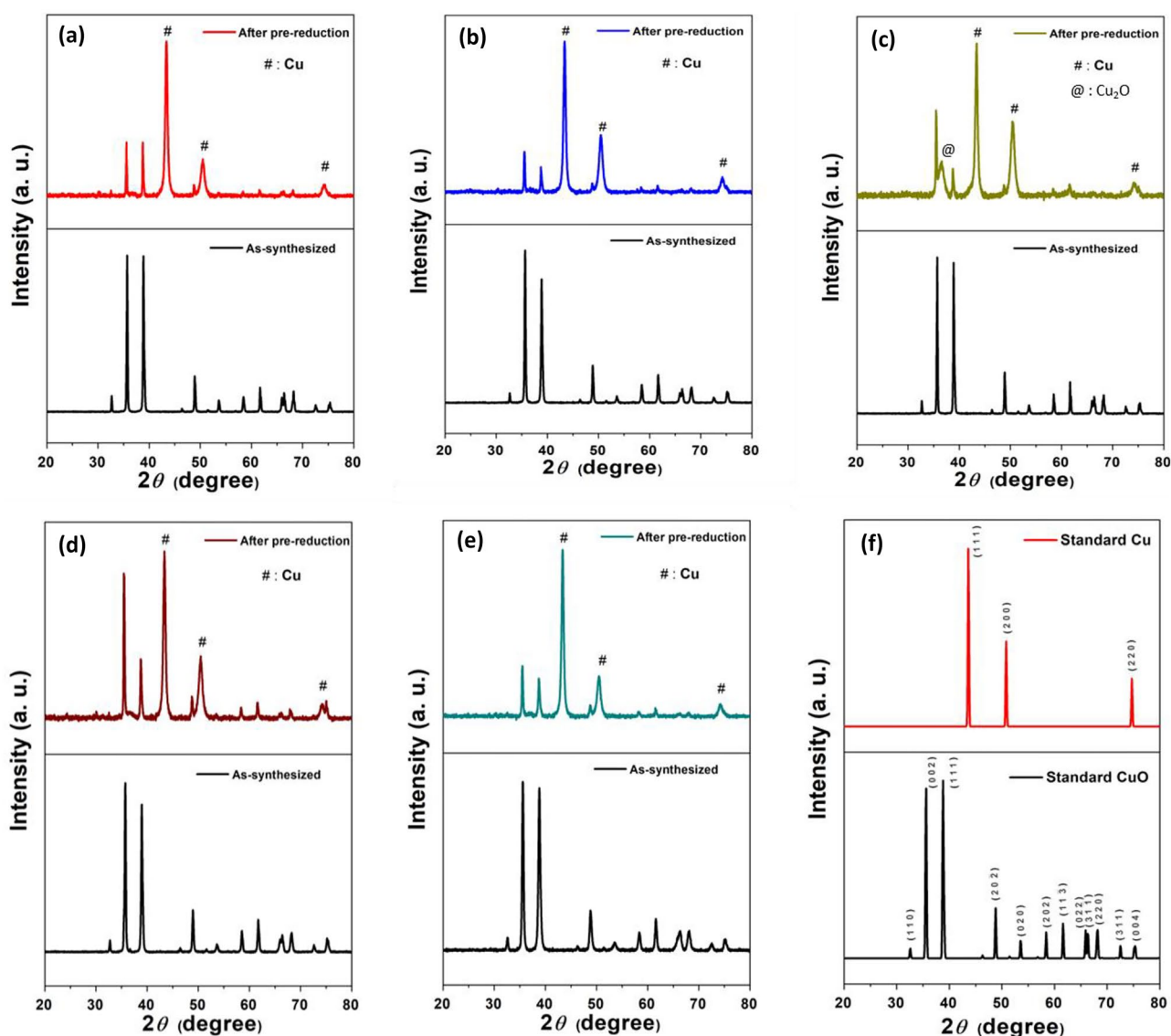


Fig. 2 X-ray diffraction patterns recorded with the CuO-based electrocatalysts in the as-synthesized and after pre-reduction step (at -0.8 V vs. RHE) conditions, for those designated as **(a)** S1, **(b)** S2, **(c)** S3, **(d)** S4,

and **(e)** S5, with **(f)** presenting the standard patterns of Cu (as per ICSD file number 7954) and CuO (as per ICSD file number 16025)

the sample types, S1, S2, S3, S4, and S5 been defined in the previous section. X-ray diffraction (XRD) data recorded with all the sample types confirm the formation of CuO, having space group C12/C1, as per ICSD-16025 database (see Fig. S3 in SI). No impurity peak could be detected within the detection limit of XRD. The lattice parameters and unit cell volumes, as estimated via Rietveld refinement of the XRD data (see Fig. S4 in SI), have been mentioned in Table 1; which tends to agree with literature reports on CuO [45–48]. XPS scans indicate the presence of Cu and O for all the samples, with the oxidation state of Cu being +2 (see Fig. S5 in SI).

Nevertheless, interesting differences could be noted in the morphologies and dimensions of the as-synthesized CuO particles, as can be seen from Fig. S6 in SI. The one prepared via solution combustion method (*viz.*, S1) exhibits fairly equiaxed morphology, with particle size of ~ 0.7 – $1\ \mu\text{m}$ (see Fig. S6a). Among those prepared via hydrothermal route (with varied conditions and/or precursors), S2 possesses a rod-shaped morphology having aspect ratio of ~ 3 – 5 (*viz.*, length ~ 3 – $5\ \mu\text{m}$ and width ~ 1 – $2\ \mu\text{m}$) (see Fig. S6b). By contrast, S3 possesses fairly equiaxed morphology, with particle size of ~ 1 – $3\ \mu\text{m}$ (*i.e.*, coarser than S1, which also possesses similar morphology) (see Fig. S6c). Interestingly, S4 presents a spherical morphology, with a relatively rough surface (more like a “cauliflower”), having particle size of ~ 2 – $3\ \mu\text{m}$ (see Fig. S6d). Different from the others, S5 exhibits needle shaped morphology with the particles being ~ 1 – $2\ \mu\text{m}$ in length, thus presenting a “grass like” appearance (see Fig. S6e). The BET specific surface areas have been found to vary between ~ 0.21 and $\sim 3.55\ \text{m}^2/\text{g}$ for the copper oxides, as presented in Fig. S7 in SI. More importantly, the electrochemically accessible surface areas, as obtained based on underpotential deposition (UPD) experiments conducted post the pre-reduction step at $-0.8\ \text{V}$ vs. RHE (see the “Underpotential Deposition of Pb on the “CuO-derived Cu” Electrocatalysts” section), indicate greater “active” surface areas for S1, S2, and S3, in comparison to those for S4 and S5 (see Fig. 1). The above aspects are likely to cast influence on the performance as electrocatalysts for eCO_2RR , as presented subsequently in the “Electrochemical CO_2 Reduction Using the “CuO-derived Cu” Electrocatalysts” section.

Copper Oxide Derived Cu

Since CuO is not thermodynamically stable under eCO_2RR conditions, prior to the bulk electrolysis experiments (*i.e.*, electrochemical CO_2 reduction; eCO_2RR), all the copper oxide electrocatalysts were first treated at a constant potential of $-0.8\ \text{V}$ vs. RHE, till stable currents were achieved; thus forming “CuO-derived Cu”. XRD data obtained after the pre-reduction step confirmed that the copper oxides got converted to copper, with strong Cu (111) and Cu (200) peaks appearing at $\sim 43.5^\circ$ and $\sim 51^\circ$, respectively (as per ICSD file

number: 7954) (see Fig. 2). No preferential crystallographic orientation or texturing of the as-formed Cu can be noted for the catalysts, with the integrated intensity ratios of the Cu (111): Cu (200) peaks varying between ~ 1.22 and 2.76 .

In addition to the peaks of Cu, residual CuO peaks can also be noted from the XRD patterns, which indicate the occurrence of partial reduction of CuO to Cu under the concerned electrochemical condition and duration. It is not ruled out here that possible oxidation of Cu upon exposure to air during handling may also be partly responsible for appearance of the CuO peaks. However, that is not likely to lead to the strong CuO peak intensities, as observed here for the pre-reduced CuOs (for comparison, see XRD pattern of micron-sized commercial Cu powder obtained after exposure to atmosphere for months; as Fig. S8 in SI). Furthermore, since exposure was minimized by storing the electrocatalyst samples in an inert atmosphere (glove-box) and also since all the samples were handled in the same way and for the same duration, the influence of air-exposure on the appearance of the CuO peaks may be neglected. Hence, the ratios of integrated intensities of Cu (111) to CuO (111), which have been presented in Fig. 3, are considered as indicators of the variations of relative contents of Cu and CuO (*i.e.*, Cu-to-CuO or Cu/CuO-contents) across the “CuO-derived Cu” electrocatalysts (*viz.*, prior to being used for the actual eCO_2RR process). Such variations may also be indicators of the kinetics associated [42, 49] with the CuO to Cu conversion at a given negative potential (here, $-0.8\ \text{V}$) for a given CuO electrocatalyst, which appears to be variable across the presently used CuOs. Here, a correlation between the surface

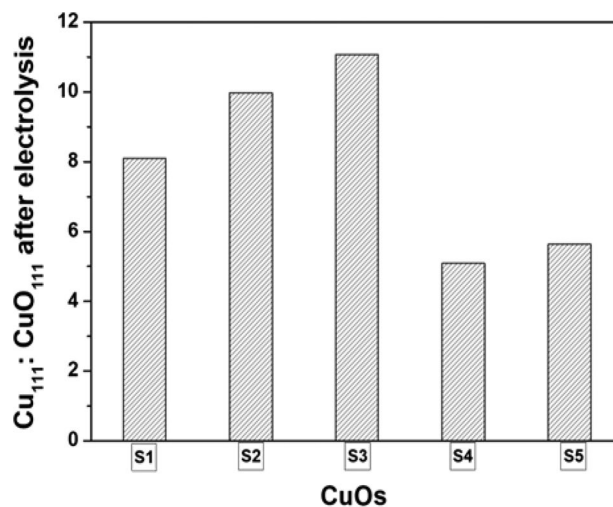


Fig. 3 The ratios of integrated intensities of the Cu(111):CuO(111) planes (as per XRD data), as an indicator of the relative Cu-to-CuO content, of the electrochemically pre-reduced CuO (partially to Cu; at $-0.8\ \text{V}$ vs. RHE), prior to eCO_2RR , for the samples designated as S1, S2, S3, S4, and S5. These indicate one of the starting/initial characteristics of the electrocatalysts prior to being used for the actual electrochemical CO_2 reduction runs

areas and the as-obtained Cu/CuO-contents of the electrocatalysts can be noted by comparing Figs. 1, 3, and S7 (in SI). The three catalysts having the higher electrochemically accessible/active surface area (as per UPD measurements), i.e., S1, S2, and S3, also possess higher Cu/CuO-contents, as compared to the S4 and S5 counterparts; with the BET surface areas also casting additional influence, as can be

realized when comparing the Cu/CuO-contents among S1, S2, and also S4, S5. More importantly, it is not unlikely that the Cu/CuO-contents, as one of the “starting” features of the CuO-based electrocatalysts used here for subsequent eCO₂RR runs, may have an influence on the performance as an electrocatalyst (see the “[Electrochemical CO₂ Reduction Using the “CuO-derived Cu” Electrocatalysts](#)” section).

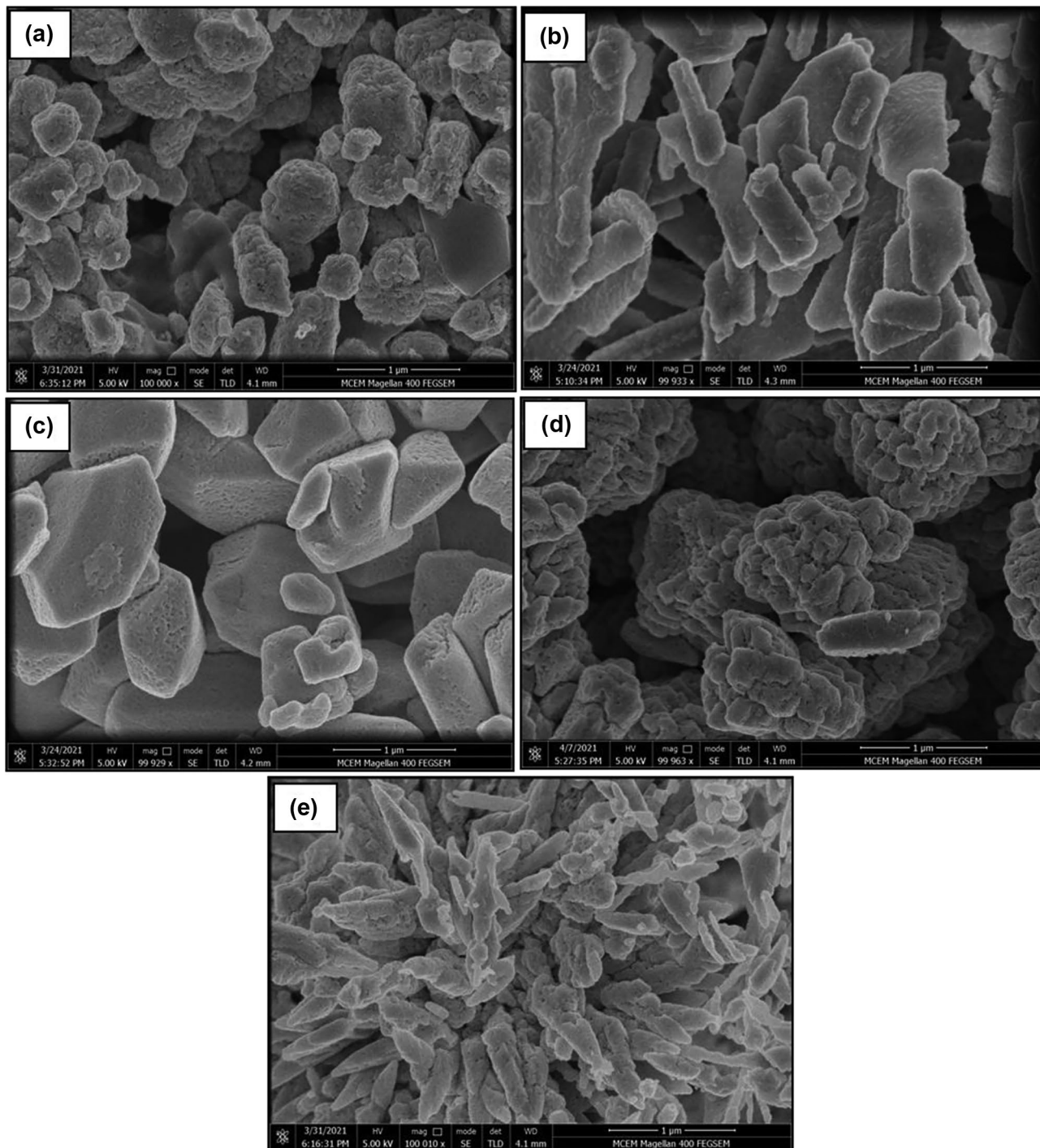


Fig. 4 SEM images of the “CuO-derived Cu” electrocatalysts, designated as (a) S1, (b) S2, (c) S3, (d) S4, and (e) S5, after the pre-reduction step (at -0.8 V vs. RHE)

SEM images obtained after the pre-reduction step at -0.8 V vs. RHE indicates that, even though the surfaces appear to be rougher, the morphology gets more or less preserved for all the electrocatalysts (see Fig. 4). Only in the case of S5, the continuous “grass like” feature appears to get discretized into a “flower like” feature (see Fig. S9i in SI). However, a closer look indicates that the basic morphology still remains the same (see Fig. S9i, j in SI). This, in a way, is also an indicator of partial reduction of CuO to Cu during the pre-reduction step at -0.8 V, since complete changeover from oxide (CuO) to metallic Cu would have altered the morphology to a significant extent.

Electrochemical CO₂ Reduction Using the “CuO-derived Cu” Electrocatalysts

Current Densities Upon Electrochemical CO₂ Reduction

Electrochemical reduction of carbon dioxide (eCO₂RR) was carried out via bulk electrolysis technique using the five types of “CuO derived Cu” electrocatalysts in H-cell (with CO₂ saturated 0.10 M KHCO₃ electrolyte; pH ~ 6.8) at six applied potentials (viz., -0.6 , -0.8 , -1.0 , -1.2 , -1.4 , and -1.6 V; vs. RHE). In terms of evolution of current densities, the eCO₂RR runs indicate that the overall current densities (as in Fig. S10a in SI), as well as those corresponding to the formation of carbon containing products (as in Fig. 5) and H₂ (as in Fig. S10b) separately, show increasing trend with potential till ~ -1.4 V, while remaining almost unchanged beyond that (viz., between -1.4 and -1.6 V) (see Fig. 5). It may be recalled here that, in addition to the different specific surface areas (see Figs. 1 and S7 in SI), the five different pre-reduced CuOs also possess different Cu-to-CuO contents (viz., $I_{\text{Cu}(111)}: I_{\text{CuO}(111)}$) primarily based on the extent of pre-reduction at -0.8 V (see Fig. 3). While the net extent of reduction of CuO to Cu can be potential dependent and the possibility of further reduction to Cu at the more negative applied potentials used during the actual electrochemical CO₂ reduction runs is not ruled out, the Cu-to-CuO content values of the pre-reduced CuOs, as used in the following discussions, is one of the “starting” conditions of the CuO-based catalysts used for the actual eCO₂RRs.

Among the electrocatalysts, the current densities associated with the formation of the carbon containing products (as in Fig. 5) are consistently higher with S1, S2, and S3, as compared to those with S4 and S5, at all the potentials. It may be recalled here that, as based on UPD measurements, the former three, i.e., S1, S2, and S3, also possess higher electrochemically accessible/active surface areas (see Fig. 1) than the S4 and S5 counterparts. This is also the case with the starting Cu-to-CuO contents (see Fig. 3). Furthermore, based on BET measurements (see Fig. S7 in SI), S2 possesses the highest specific surface area. Hence,

it is likely that a combination of these aspects results in S2 yielding the highest current density for the C-containing product formations during eCO₂RR. Hence, the present set of results points towards an interesting interplay between the specific surface area and the starting Cu-content (viz., the active sites) of “CuO derived Cu” electrocatalysts towards the activity in the context of eCO₂RR.

Products Obtained Upon Electrochemical CO₂ Reduction

The gaseous products (as detected by GC-TCD, GC-FID) and liquid products (as detected by NMR) of eCO₂RR obtained in this study include CO, C₂H₄, CH₄, H₂, formate (HCOO⁻), acetate (CH₃COO⁻), C₂H₅OH, and n-propanol (in relatively smaller amount). The variations of faradaic efficiencies (FE; as %) corresponding to the products with applied potentials, as obtained with the different CuO-based electrocatalysts, have been presented in Fig. 6. On a different note, cyclic voltammograms obtained with the “CuO-derived Cu” electrocatalysts under consideration here, prior to and post usage for the eCO₂RR runs, have been presented in Fig. S11 in SI.

For the product formations, as is fairly usual, the FE for hydrogen production increased, while that for CO decreased, with increasing potential in the negative direction for all the five “CuO derived Cu” electrocatalysts. Nevertheless, one may note that S2 (having the second highest specific surface area), S1, S2, and S3 (having high Cu-to-CuO content) dominate the faradaic efficiency for CO evolution. During the electrochemical CO₂ reduction runs, CO got further reduced to methane and C₂ (ethylene, ethanol) products [14]. Here, it may be noted that, among the five electrocatalysts,

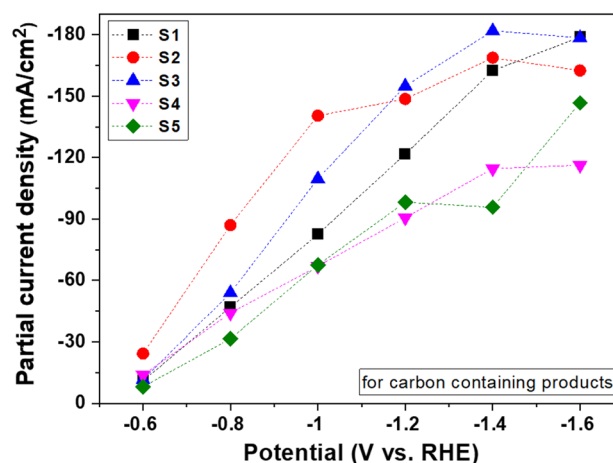


Fig. 5 The variations of current densities associated with the formation of carbon (C) containing products upon electrochemical CO₂ reduction at the applied potentials of -0.6 , -0.8 , -1.0 , -1.2 , -1.4 , and -1.6 V (vs. RHE) using the “CuO-derived Cu” electrocatalysts, designated as S1, S2, S3, S4, and S5. The C-containing products obtained in this study include CO, C₂H₄, CH₄, formate (HCOO⁻), acetate (CH₃COO⁻) and C₂H₅OH

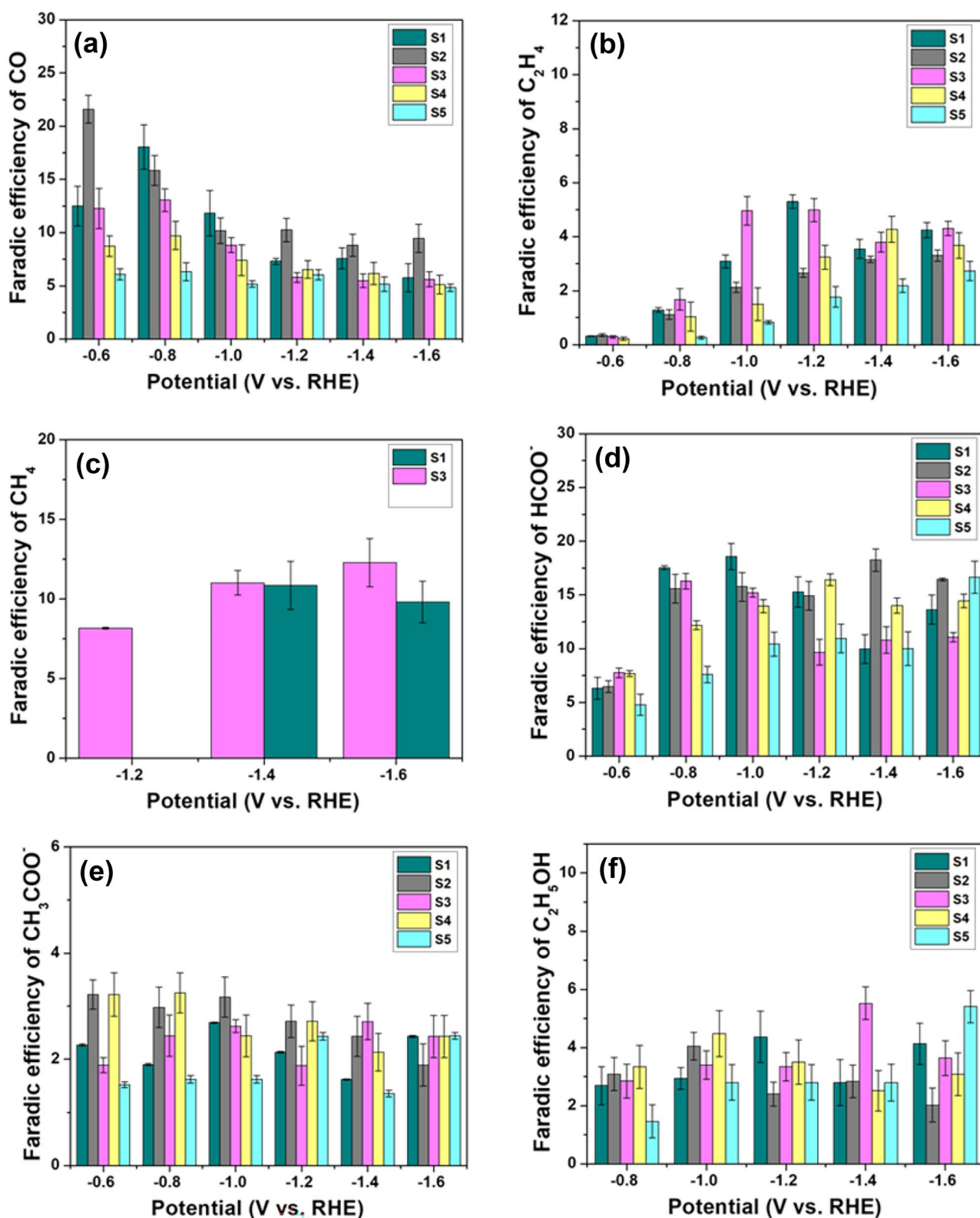


Fig. 6 Faradaic efficiencies (as %) associated with the formation of gaseous and liquid products, viz., (a) carbon monoxide (CO), (b) ethylene (C₂H₄), (c) methane (CH₄), (d) formate (HCOO⁻), (e) acetate (CH₃COO⁻), (f) ethanol (C₂H₅OH), upon electrochemical CO₂ reduction using the

as-developed “CuO-derived Cu” electrocatalysts (designated as, S1, S2, S3, S4, S5) at the potentials of -0.6 V, -0.8 V, -1.0 V, -1.2 V, -1.4 V, and -1.6 V vs. RHE

only S1 led to the formation of all the seven types of products; viz., CO, C₂H₄, CH₄, HCOO⁻, CH₃COO⁻, C₂H₅OH, and small amount of n-propanol. Furthermore, it is only S1 and S3, i.e., the two electrocatalysts having high “starting” Cu-to-CuO contents (i.e., post pre-reduction step) but low specific surface area (see Figs. 1 and 3), that led to the formation of methane (CH₄), albeit only at the greater negative potentials (viz., beyond -1.0 V). Also, for almost all the products, it is primarily S1, S2, and S3 (having the higher Cu-to-CuO contents; see Fig. 3) that led to higher faradaic efficiencies at the lower negative potentials. S5, having the highest specific surface area, but relatively low Cu-content, consistently resulted in the lowest FE (at the lower negative potentials). These are despite the current densities being on the lower side for S1 and S3 (in fact, lowest for S1) at the lesser negative potentials, which is believed to be a more direct manifestation of their relatively lower specific surface areas. Again, the faradaic efficiencies and product formation were found to be governed, to a good extent, by the “starting” Cu-to-CuO contents of the CuO-based electrocatalysts used. Nevertheless, at the greater negative potentials, the bias with respect to the relative Cu/CuO-content (i.e., the influence of Cu-to-CuO content) tends to go down for some of the products (like formate, acetate, and ethanol), which may possibly be due to considerably greater extent of CuO to Cu conversion of the catalysts themselves at the more negative potentials. Overall, along with the results for current density (as discussed in the “Current Densities Upon Electrochemical CO₂ Reduction” section and presented in Fig. 5), the above observations further highlight the importance of relative Cu/CuO-content (and, thus, “active sites” [31]) in “CuO-derived Cu” electrocatalysts for usage in eCO₂RR; especially at less negative potentials.

In the context of variations of faradaic efficiencies for the different types of products with potentials, it can be observed that at the potential of -0.6 V, FE of CO was the highest, while that of C₂H₄ was the lowest for all the electrocatalysts (see Figs. 6a, b). Furthermore, moving to more negative potentials (i.e., from -0.8 to -1.6 V; vs. RHE), in general, the FE of CO shows a decreasing trend and that of C₂H₄ shows increasing trend. Talking about the major product, it was CO at the potentials of -0.6 and -0.8 V (vs. RHE) (with maximum FE of $\sim 21.6 \pm 1.3\%$ at -0.6 V for S2) and formate at the other four potentials (viz., -1.0, -1.2, -1.4, -1.6 V; vs. RHE) (with maximum FE of $\sim 18.6 \pm 1.2\%$ at -1.0 V for S1).

Conclusion

CuO electrocatalysts for electrochemical CO₂ reduction reaction (eCO₂RR) were synthesized with five different types of morphologies and specific surface areas via solution combustion

and hydrothermal synthesis routes (with varied conditions). Prior to CO₂ reduction via bulk electrolysis at six different potentials (viz., -0.6, -0.8, -1.0, -1.2, -1.4, and -1.6 V; vs. RHE), the CuO catalysts were first electrochemically reduced (at -0.8 V; vs. RHE) to form “CuO-derived Cu”, but with varying Cu-to-CuO contents, which are considered here as starting conditions of the electrocatalysts. With respect to the products of eCO₂RR, in addition to H₂ evolution, a total of seven liquid and gaseous products, viz., CO, C₂H₄, CH₄, formate (HCOO⁻), acetate (CH₃COO⁻), C₂H₅OH, were detected; the faradaic efficiencies of which were found to depend not only on the potentials, but also on the types of “CuO-derived Cu” electrocatalysts used.

In the context of current densities, product formations and associated faradaic efficiencies (FEs), not only the specific surface area, but also the relative content of Cu with respect to CuO obtained prior to the eCO₂RR process (viz., the “starting” Cu:CuO-content) seemingly played an important role. In general, the ones having relatively higher starting Cu/CuO-contents (and, thus, “active sites”) resulted in higher current densities associated with the formation of the carbon containing products and higher corresponding faradaic efficiencies, especially at the lower negative potentials. Furthermore, only two electrocatalysts having the higher starting Cu-to-CuO contents led to the formation of methane (CH₄), albeit only at greater negative potentials (viz., beyond -1.0 V). In fact, both the concerned CuOs possess simple equiaxed morphologies, as against any special rod/whisker-type morphology. Accordingly, by developing and using “CuO-derived Cu” electrocatalysts possessing different morphologies (thus, different specific surface areas) and varied initial Cu-to-CuO contents (prior to the eCO₂RR process), the present work throws important insights into the relative roles of, as well as interplay between, specific surface area and starting Cu/CuO-content on the current densities, product formation and associated faradaic efficiencies upon electrochemical CO₂ reduction.

Supplementary Information The online version contains supplementary material available at <https://doi.org/10.1007/s12678-023-00814-1>.

Acknowledgements The authors are grateful to the School of Chemistry, Monash University, for allowing the usage of XRD, NMR, GC-TCD, and GC-FID facilities. MB is grateful to the Central Facility of Monash University for allowing the usage of SEM. She is also grateful to the Department of Chemical Engineering, IIT Bombay for allowing the usage of BET and to ICCF, IRCC, IIT Bombay for allowing the usage of X-ray photoelectron spectroscopy (ESCA). She is grateful to the IITB-Monash Research Academy for the financial support during her doctoral study (IMURA0620). AS acknowledges the Department of Science and Technology, Government of India (DST/TM/EWO/MI/CCUS/18 (C1)) for the financial support provided for sample characterization.

Declarations

Conflict of Interest The authors declare no competing interests.

References

- Y. Hori, H. Wakebe, T. Tsukamoto, O. Koga, *Electrochim. Acta* **39**, 1833 (1994)
- D. Johnson, Z. Qiao, A. Djire, *ACS Appl. Energ. Mater.* **4**, 8661 (2021)
- K.P. Kuhl, T. Hatsukade, E.R. Cave, D.N. Abram, J. Kibsgaard, T.F. Jaramillo, *J. Am. Chem. Soc.* **136**, 14107 (2014)
- E.R. Cave, C. Shi, K.P. Kuhl, T. Hatsukade, D.N. Abram, C. Hahn, K. Chan, T.F. Jaramillo, *ACS Catal.* **8**, 3035 (2018)
- K.P. Kuhl, E.R. Cave, D.N. Abram, T.F. Jaramillo, *Energy Environ. Sci.* **5**, 7050 (2012)
- J.T. Feaster, C. Shi, E.R. Cave, T. Hatsukade, D.N. Abram, K.P. Kuhl, C. Hahn, J.K. Norskov, T.F. Jaramillo, *ACS Catal.* **7**, 4822 (2017)
- C. Xiao, J. Zhang, *ACS Nano* **15**, 7975 (2021)
- Z. Ni, H. Liang, Z. Yi, R. Guo, C. Liu, Y. Liu, H. Sun, X. Liu, *Coord. Chem. Rev.* **441**, 213983 (2021)
- Z. Tao, Z. Wu, X. Yuan, Y. Wu, H. Wang, *ACS Catal.* **9**, 10894 (2019)
- D. Ren, Y. Deng, A.D. Handoko, C.S. Chen, S. Malkhandi, B.S. Yeo, *ACS Catal.* **5**, 2814 (2015)
- C. Zhan, F. Dattila, C. Rettenmaier, A. Bergmann, S. Kuhl, R.G. Muelas, N. Lopez, B.R. Cuenya, *ACS Catal.* **11**, 7694 (2021)
- X. Yao, Y. Guo, B. Liu, P. Wang, J. Sun, W. Li, C. Zhao, *ChemElectroChem* **8**, 592 (2021)
- A.W. Khasay, K.B. Ibrahim, M.C. Tsai, M.K. Birhanu, S.A. Chala, W.N. Su, B.J. Hwang, *Catal. Lett.* **149**, 860 (2019)
- S. Chu, S. Hong, J. Masa, X. Li, Z. Sun, *ChemComm* **55**, 12380 (2019)
- Y. Lan, G. Niu, F. Wang, D. Cui, Z. Hu, *A.C.S. Appl. Mater. Interfaces* **12**, 36128 (2020)
- Y. Li, S. Chu, H. Shen, Q. Xia, A.W. Robertson, J. Masa, U. Siddiqui, Z. Sun, *A.C.S. Sustain. Chem. Eng.* **8**, 4948 (2020)
- Y. Jiang, C. Choi, S. Hong, S. Chu, T.S. Wu, Y.L. Soo, L. Hao, Y. Jung, Z. Sun, *Cell Rep. Phys. Sci.* **2**, 100356 (2021)
- S. Lee, D. Kim, J. Lee, *Angew. Chem. Int. Ed.* **54**, 14701 (2015)
- J. Xie, Y. Huang, H. Yu, *Front. Environ. Sci. Eng.* **9**(5), 861 (2015)
- L. Mandal, K. R. Yang, M. R. Motapothula, D. Ren, P. Lobaccaro, A. Patra, M. Sherburne, V. S. Batista, B. S. Yeo, J. W. Ager, J. Martin, T. Venkatesan, *ACS Appl. Mater. Interfaces* **10**, 8574 (2018)
- Y. Wang, C. Niu, Y. Zhu, D. He, W. Huang, *A.C.S. Appl. Mater. Interfaces* **3**, 9841 (2020)
- J. Kim, W. Choi, J.W. Park, C. Kim, M. Kim, H. Song, *J. Am. Chem. Soc.* **141**, 6986 (2019)
- M. Ma, K. Djanashvili, W.A. Smith, *Phys. Chem. Chem. Phys.* **17**, 20861 (2015)
- A.M. Asiri, J. Gao, S.B. Khan, K.A. Alamry, H.M. Marwani, M.S.J. Khan, W.A. Adeosun, S.M. Zakeeruddin, D. Ren, M. Gratzel, *J. Phys. Chem. Lett.* **13**, 345 (2022)
- A. Loiudice, P. Lobaccaro, E.A. Kamali, T. Thao, B.H. Huang, J.W. Ager, R. Buonsanti, *Angew. Chem. Int. Ed.* **55**, 5789 (2016)
- D. Gao, I. Zegkinoglou, N.J. Divins, F. Scholten, I. Sinev, P. Grosse, B.R. Cuenya, *ACS Nano* **11**, 4825 (2017)
- C.S. Chen, A.D. Handoko, J.H. Wan, L. Ma, D. Ren, B.S. Yeo, *Catal. Sci. Technol.* **5**, 161 (2015)
- F.S. Ke, X.C. Liu, J. Wu, P.P. Sharma, Z.Y. Zhou, J. Qiao, X.D. Zhou, *Catal. Today* **288**, 18 (2017)
- P. Qi, L. Zhao, Z. Deng, S. Hao, H. Li, Q. Liu, X. Li, Y. Lian, J. Cheng, J. Guo, Y. Cui, Y. Peng, *J. Phys. Chem. Lett.* **12**, 3941 (2021)
- Y. Lan, S. Ma, J. Lu, P.J.A. Kenis, *Int. J. Electrochem. Sci.* **9**, 7300 (2014)
- L. Wang, K. Gupta, J.B.M. Goodall, J.A. Darr, K.B. Holt, *Faraday Discuss.* **197**, 517 (2016)
- T. Moller, F. Scholten, T.N. Thanh, I. Sinev, J. Timoshenko, X. Wang, Z. Jovanov, M. Gliech, B.R. Cuenya, A.S. Varela, P. Strasser, *Angew. Chem. Int. Ed.* **59**, 17974 (2020)
- H. Mistry, A.S. Varela, C.S. Bonifacio, L. Zegkinoglou, L. Sinev, Y.W. Choi, K. Kisslinger, E.A. Stach, J.C. Yang, P. Strasser, B.R. Cuenya, *Nature Commun.* **7**, 12123 (2016)
- A.H. Shah, Y. Wang, S. Hussain, M.B. Akbar, A.R. Woldu, X. Zhang, T. He, *Phys. Chem. Chem. Phys.* **22**, 2046 (2020)
- C.W. Li, M.W. Kanan, *J. Am. Chem. Soc.* **134**, 7231 (2012)
- A.D. Handoko, C.W. Ong, Y. Huang, Z.G. Lee, L. Lin, G.B. Panetti, B.S. Yeo, *J. Phys. Chem. C* **120**, 20058 (2016)
- R. Kas, R. Kortlever, A. Milbrat, M.T.M. Koper, G. Mul, J. Baltrusaitis, *Phys. Chem. Chem. Phys.* **16**, 12194 (2014)
- T.-D. Nguyen-Phan, C. Wang, C.M. Marin, Y. Zhou, E. Stavitski, E.J. Popczun, Y. Yu, W. Xu, B.H. Howard, M.Y. Stuckman, I. Waluyo, P.R. Ohodnicki Jr., D.R. Kauffman, *J. Mater. Chem. A* **7**, 27576 (2019)
- P. Liu, H. Liu, S. Zhang, J. Wang, C. Wang, *Electrochim. Acta* **354**, 136753 (2020)
- L.R.L. Ting, R.G. Muelas, A.J. Martin, F.L.P. Veenstra, S.T.J. Chen, Y. Peng, E.Y.X. Per, S.P. Garcia, N. Lopez, J.P. Ramirez, B.S. Yeo, *Angew. Chem. Int. Ed.* **132**, 21258 (2020)
- S.D. Giri, A. Sarkar, S.M. Mahajani, v Suresh, *ECS Trans.* **75**(48), 19 (2017)
- Y. Lan, C. Gai, P.J.A. Kenis, J. Lu, *ChemElectroChem* **1**, 1577 (2014)
- S.D. Giri, A. Sarkar, *Adv. Powder Technol.* **29**, 3520 (2018)
- S.D. Giri, S.M. Mahajani, A.K. Suresh, A. Sarkar, *Mater. Res. Bull.* **123**, 110702 (2020)
- L.V. Devi, T. Selvalakshmi, S. Sellaiyan, A. Uedono, K. Sivaji, S. Sankar, *J. Alloy. Compd.* **709**, 496 (2017)
- A.K. Mishra, A. Roldan, N.H.D. Leeuw, *J. Phys. Chem. C* **120**, 2198 (2016)
- D. Su, X. Xie, S. Dou, G. Wang, *Sci. Rep.* **4**, 5753 (2014)
- M.Z. Sahdan, M.F. Nurfazliana, S.A. Kamaruddin, Z. Embong, Z. Ahmad, H. Saim, *Procedia Manufacturing* **2**, 379 (2015)
- H. Xiao, W.A. Goddard III., T. Cheng, Y. Liu, *PNAS* **114**, 6685 (2017)

Publisher's Note Springer Nature remains neutral with regard to jurisdictional claims in published maps and institutional affiliations.

Springer Nature or its licensor (e.g. a society or other partner) holds exclusive rights to this article under a publishing agreement with the author(s) or other rightsholder(s); author self-archiving of the accepted manuscript version of this article is solely governed by the terms of such publishing agreement and applicable law.